Soils and Rocks
An International Journal of Geotechnical and Geoenvironmental Engineering
www.soilsandrocks.com
ISSN 1980-9743
ISSN-e 2675-5475

Stress-path dependency and anisotropy in cemented iron ore tailings: insights from laboratory assessment

Gustavo Dias Miguel[1#], Vinícius Batista Godoy[1], Lucas Festugato[1]

Article

Keywords
Ground improvement
Iron ore tailings
Stress-path dependency
Intermediate principal stress
Anisotropy
Cemented tailings

Abstract

The mechanical behaviour of filtered iron ore tailings is governed by stress paths and fabric anisotropy induced during placement and compaction in "dry"-stacked facilities. Although cementation is widely used to enhance strength and stiffness, most studies remain limited to axisymmetric conditions, providing limited insight into multiaxial stress states and the role of intermediate principal stress. This study evaluates the multiaxial behaviour of cemented iron ore tailings under different stress paths, focusing on stress-path dependency and anisotropy. Initial characterization comprised unconfined compression tests on mixtures prepared with varying dry unit weights and cement contents. Selected mixtures were then tested in a true triaxial apparatus under constant mean effective stress, considering compression, plane stress, and extension loading paths. Results show that cementation increases stiffness and strength while reducing sensitivity to loading direction and stress path. Compaction-induced anisotropy observed in untreated tailings is mitigated after cement addition, particularly under compression and plane stress conditions. Cemented specimens also exhibit lower volumetric strains, indicating improved resistance to contractive behaviour. Overall, cementation promotes a more isotropic multiaxial response in iron ore tailings under stress conditions representative of "dry"-stacked facilities, highlighting the importance of incorporating stress-path effects in stability assessments.

1. Introduction

Mining activities support industrial development and economic growth worldwide. In Brazil, the sector accounts for approximately 3% of gross domestic product, and the country has ranked among the largest iron ore producers in recent years (Instituto Brasileiro de Mineração, 2020). In Botswana, mining may represent up to 40% of national gross domestic product (Ministry of Foreign Affairs of Brazil, 2021). Declining ore grades and increasing production have generated progressively larger quantities of tailings, fine-grained residues produced during the extraction and beneficiation of low-grade ores (Kossoff et al., 2014).

Mining tailings are man-made geomaterials composed mainly of finely crushed rock, residual minerals and processing chemicals. Their fabric, grading and mechanical response depend strongly on beneficiation and disposal methods. Commonly deposited under saturated or near-saturated conditions, tailings have been associated with stability problems in containment structures, including large-scale failures (Morgenstern et al., 2016; Robertson et al., 2019). Such events demonstrate that concepts developed for natural soils may not fully capture tailings behaviour, reinforcing the need for dedicated experimental investigation.

Filtered-tailings disposal in piles, commonly referred to as "dry" stacking, has emerged as an alternative to conventional tailings dams. Improved control of water content and compaction may enhance operational safety (Lupo & Hall, 2010). However, "dry"-stacked tailings facilities are typically constructed in zones with different deposition sequences, compaction efforts and material conditioning (Davies et al., 2011). They are therefore inherently heterogeneous, with spatial variations in density, stiffness and fabric that may cause differential settlements and expose the material to non-axisymmetric stress states, in which intermediate principal stress and loading direction influence the mechanical response.

Binder- and fibre-based stabilisation techniques have been investigated to improve loosely compacted or less structured zones within "dry"-stacked tailings facilities. Cementation and fibre reinforcement significantly increase the strength and stiffness of gold tailings under monotonic and cyclic loading, although damage to the cemented matrix may occur (Festugato et al., 2013, 2015). The benefits of cementation in soils and granular materials are well established, and rational dosage methods based on the porosity-to-volumetric cement

#Corresponding author. E-mail address: gustavodiasmiguel@gmail.com
[1]Universidade Federal do Rio Grande do Sul, Programa de Pós-graduação em Engenharia Civil, Porto Alegre, RS, Brasil.

Submitted on July 18, 2026; Final Acceptance on October 2, 2026; Discussion open until February 28, 2027.
Editor: Renato P. Cunha
https://doi.org/10.28927/SR.2026.010326

This is an Open Access article distributed under the terms of the Creative Commons Attribution license (https://creativecommons.org/licenses/by/4.0/), which permits unrestricted use, distribution, and reproduction in any medium, provided the original work is properly cited.

content index have been widely adopted (Consoli et al., 2007, 2010, 2019). For iron ore tailings, this index controls unconfined compressive strength, small-strain stiffness and liquefaction resistance under conventional triaxial loading (Consoli et al., 2022).

Despite these advances, studies of cemented tailings and soils have largely focused on uniaxial or axisymmetric conditions. Under multiaxial stress states, geomaterial behaviour is strongly influenced by intermediate principal stress and loading direction, commonly described by the Lode angle. For uncemented sands and soils, inherent and induced anisotropy associated with deposition and compaction has been extensively documented, with stiffness, strength and volumetric response depending on stress path and fabric orientation (Parkin et al., 1968; Arthur & Menzies, 1972; Oda & Koishikawa, 1979; Fioravante & Capoferri, 2001). However, how cementation modifies stress-path dependency and compaction-induced anisotropy in fine-grained iron ore tailings remains insufficiently understood.

This study investigates the multiaxial mechanical behaviour of cemented iron ore tailings under different stress paths. Its main novelty is the systematic use of true triaxial testing to assess how cementation modifies the combined effects of intermediate principal stress, loading direction and compaction-induced anisotropy under compression, plane-stress and extension conditions, which remain scarcely investigated for fine-grained cemented tailings. The experimental programme combines unconfined compression and true triaxial testing. This framework evaluates stress-path and fabric-orientation effects on stiffness, strength and volumetric response within a consistent cement-porosity-based approach. The results provide new experimental evidence on the extent to which cementation suppresses directional dependence under multiaxial loading and support the analysis and performance assessment of "dry"-stacked tailings facilities.

2. Experimental programme

The experimental programme was designed to investigate the mechanical behaviour of cemented iron ore tailings under both conventional and multiaxial loading conditions. The programme was divided into two complementary phases. Phase I comprised unconfined compression tests performed to evaluate the influence of dry unit weight and cement content on compressive strength and to define suitable mixtures for multiaxial testing. Phase II consisted of true triaxial tests carried out under controlled stress paths, allowing the effects of intermediate principal stress and loading direction to be systematically assessed.

2.1 Phase I – Unconfined compression testing

Phase I included unconfined compression tests performed on cylindrical specimens. These tests were conducted over a wide range of dry unit weights (17.5, 19.0, 20.5 and 22.0 kN/m^3) and ordinary Portland cement contents (3%, 5% and 7%, by dry mass of tailings). The objective of this phase was not only to characterise the mechanical response of the tailings–cement blends, but also to identify mixtures exhibiting low absolute strength levels compatible with the operational limits of the true triaxial apparatus. The Phase I experimental setup is summarized in Table 1.

The Phase I results were used to establish the relationship between unconfined compressive strength and the porosity-to-volumetric cement content index, enabling the selection of target mixtures for Phase II. In particular, mixtures yielding unconfined compressive strengths of approximately 180 kPa were selected to ensure that multiaxial tests could be conducted without exceeding equipment constraints, while still allowing the effects of cementation on stress-path dependency and anisotropy to be investigated.

2.2 Phase II – Multiaxial testing framework

Phase II comprised true triaxial tests performed on cubical specimens with 100 mm sides. A total of twenty-one specimens were tested, including fourteen cemented and seven untreated tailings specimens. Cemented specimens were prepared using two selected mixtures, corresponding to dry unit weights of 16.5 and 17.5 kN/m^3 and cement contents of 4.38% and 2.66%, respectively. These mixtures were chosen based on Phase I results to achieve similar unconfined compressive strength levels while maintaining different combinations of porosity and cement content. The Phase II experimental setup is summarized in Table 2.

All true triaxial tests were conducted under a constant mean effective stress of 100 kPa, adopted to facilitate comparison between stress paths and to limit the number of test variables. The loading programme explored three values of the intermediate principal stress parameter, b, corresponding to compression ($b = 0$), plane stress ($b = 0.5$) and extension ($b = 1$) conditions. For each b value, tests were performed at different loading directions, defined by the Lode angle θ, allowing the influence of loading orientation relative to the compaction direction to be evaluated.

Table 1. Phase I experimental set up.

Test type	Controlled factors	Constant factors	Experimental runs
UCS	γ_d = 17.5, 19.0, 20.5 and 22.0 kN/m^3	Materials: soil matrix and OPC; Curing time: 7 days	36
	C = 3, 5 and 7%	Curing temperature: 23±2ºC Moisture content: 11.3%	

Table 2. Phase II experimental set up.

Test type	θ (°)	Controlled factors	$\eta/C_{iv}^{0.16}$	Constant factors	Runs
True triaxial	0, 30, 60, 90, 120, 150 and 180	γ_d = 17.5 kN/m³	-	Materials: soil matrix	7
		C = 0.00%		p' = 100 kPa	
		γ_d = 16.5 kN/m³	42.40	Materials: soil matrix and OPC	7
		C = 4.38%		Curing time: 7 days	
		γ_d = 17.5 kN/m³		Curing temperature: 23±2ºC	7
		C = 2.66%		p' = 100 kPa	

2.3 Stress paths and loading directions

During true triaxial testing, the three principal stresses were prescribed at constant mean effective stress. The intermediate principal stress parameter, b, was defined as the ratio of the intermediate-to-minor stress difference to the major-to-minor stress difference, while the Lode angle θ described stress-path orientation on the deviatoric plane.

For b = 0, axisymmetric compression was imposed by increasing the major principal stress while maintaining equal intermediate and minor stresses. For b = 0.5, plane-stress paths were applied with the intermediate principal stress held constant. For b = 1, extension-dominated paths were imposed with equal major and intermediate stresses. Different θ values were adopted to evaluate loading orientation relative to the specimen compaction axis.

This framework enabled the combined effects of cementation, intermediate principal stress and loading direction on stiffness, strength and volumetric response to be assessed under conditions representative of "dry"-stacked tailings facilities.

3. Materials

Iron ore tailings were obtained from the Quadrilátero Ferrífero region of Minas Gerais, Brazil, where iron-rich metamorphic formations, mainly itabirite, are extensively mined (Pereira, 2005). Beneficiation produces fine-grained tailings dominated by silt- and clay-sized particles.

The material had liquid and plastic limits of 27% and 18%, respectively, resulting in a plasticity index of 9% and classification as low-plasticity clay (CL) under the Unified Soil Classification System. The specific gravity of solids was 3.18, and the hygroscopic moisture content was 2.92%. The particle-size distribution comprised 1.00% medium sand, 16.45% fine sand, 54.87% silt and 27.68% clay, with no gravel or coarse sand and a median particle diameter, D_{50}, of 0.021 mm. Testing followed ASTM D4318 (ASTM, 2017b), ASTM D854 (ASTM, 2014), ASTM D6913/D6913M (ASTM, 2017c) and ASTM D2487 (ASTM, 2017a), as applicable.

As shown in Figure 1, the particle-size distribution was consistent with literature data for tailings generated by similar beneficiation processes. The material had an alkaline *pH* of 8.6, determined according to ASTM D4972 (ASTM, 2019), and maximum and minimum void ratios of 1.450 and 0.440, respectively. The maximum void ratio was obtained using an adapted ASTM D4254 (ASTM, 2016) procedure, and these values supported the selection of the dry unit weights adopted in the study.

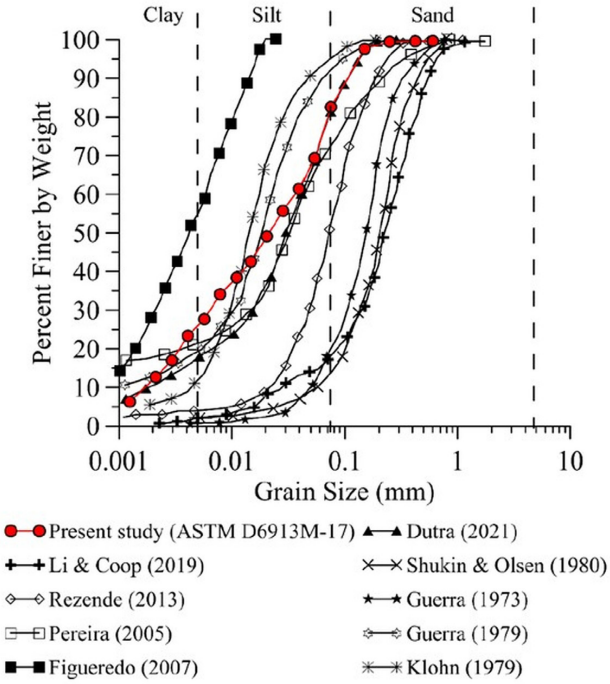


Figure 1. Particle-size distribution of the investigated iron ore tailings compared with literature data (Guerra, 1973, 1979; Klohn, 1979; Shukin & Olsen, 1980; Pereira, 2005; Figueredo, 2007; Rezende, 2013; Li & Coop, 2019; Dutra, 2021).

High-early-strength ordinary Portland cement was used as the stabilising agent. The cement was classified as Type III according to ASTM C150 (ASTM, 2012) and equivalent to CP V-ARI under ABNT NBR 5733 (ABNT, 2018), promoting strength development within the selected curing periods. Distilled water was used to control moisture content and minimise variability associated with water chemistry.

4. Methods

4.1 Sample preparation and curing

Phase I tests were performed on cylindrical specimens with 50 mm diameter and 100 mm height. Four dry unit weights (17.5, 19.0, 20.5 and 22.0 kN/m^3) and three cement contents (3%, 5% and 7%, by dry mass of tailings) were investigated. The selected dry unit weights were defined based on the modified energy Proctor compaction tests [56,000 ft-lbf/ft^3 (2,700 kN-m/m^3), ASTM D1557 (ASTM, 2021b)], which indicated an optimum moisture content of 11.3% and a maximum dry unit weight of approximately 22.0 kN/m^3. Cement contents were selected following established international practice for cemented soils and tailings, as documented in previous studies (Mitchell, 1981; Consoli et al., 2007, 2010, 2016, 2019; Festugato et al., 2013, 2019; Corte et al., 2019; Menger et al., 2022; Silva et al., 2022; Scheuermann Filho et al., 2022a; Pasche et al., 2022).

Phase II true triaxial tests were performed on 100 mm cubic specimens. Based on the Phase I results, two cemented mixtures were selected, with dry unit weight–cement content combinations of 16.5 kN/m^3–4.38% and 17.5 kN/m^3–2.66%. Both mixtures corresponded to $\eta/C_{iv}^{0.16} \approx 42.40$ and exhibited unconfined compressive strengths of approximately 180 kPa, within the operational capacity of the true triaxial apparatus. Untreated tailings specimens prepared at γ_d = 17.5 kN/m^3 were also tested for comparison.

Specimen preparation consisted of weighing the required amounts of tailings and ordinary Portland cement, followed by dry mixing until a homogeneous blend was obtained. Distilled water was then added to achieve the target moisture content of 11.3%, and mixing continued until uniform consistency was achieved. Specimens were prepared by static compaction using the moist tamping technique with a hydraulic jack and reaction frame. Each specimen was compacted in three layers, and the surface of each layer was lightly scarified before placing the subsequent layer to minimise interlayer discontinuities. The compaction procedure defined a preferential fabric orientation, with the compaction direction aligned with the vertical axis of the specimen.

A curing period of seven days was adopted for all cemented specimens in both phases of the experimental programme. During curing, specimens were stored in a climate-controlled room at a temperature of 20 ± 2 °C and relative humidity of approximately 95%. On the sixth day, cemented specimens were submerged in distilled water for 24 hours prior to testing, aiming to minimise suction effects, following procedures adopted in previous studies (Consoli et al., 2011, 2020a, 2020b, 2021a, 2021b; Carretta et al., 2020; Andreghetto et al., 2022; Festugato et al., 2023; Miguel et al., 2021, 2022a, 2022b, 2023; Queiroz et al., 2022; Scheuermann Filho et al., 2022b).

4.2 Unconfined compression tests

Unconfined compression tests were conducted in accordance with ASTM C39 (ASTM, 2021a). The tests were performed using a loading frame with a maximum capacity of 50 kN, equipped with a 10 kN load cell with a resolution of 0.005 kN. Axial loading was applied at a constant displacement rate of 1.14 mm/min. For each mixture and compaction condition, three specimens were tested to reduce experimental variability, and the reported results correspond to average values.

4.3 True triaxial tests

True triaxial tests were performed using an automated stress-controlled apparatus developed at the Federal University of Rio Grande do Sul, which independently controls the three principal stresses on cubical specimens through rigid–flexible boundaries (Andreghetto, 2022; Andreghetto et al., 2022).

The procedure comprised carbon dioxide flushing, backpressure saturation with distilled water, isotropic consolidation and shearing on the seventh day of curing. Before saturation, specimens were installed in the chamber with paper-based filters and top-hat-shaped membranes to facilitate fluid circulation.

Because of the relatively high stiffness of the cemented specimens, a mixed rigid–flexible boundary configuration was adopted, as in previous studies (Silvani et al., 2022; Festugato et al., 2023). Flexible rubber membranes formed the loading faces, while rigid aluminium plates formed the restrained faces, reducing specimen rotation and stabilising stress application.

During shearing, the mean effective stress was maintained at 100 kPa, with stress increments or decrements applied at 2 kPa/min. Tests ended upon specimen or membrane failure, or when the minor principal stress approached the backpressure level to prevent damage to the displacement transducers.

5. Results and discussion

5.1 Unconfined compressive strength and selection of Phase II mixtures

The unconfined compression results confirm that the mechanical behaviour of cemented iron ore tailings is governed by the combined effects of porosity and cement content, which can be consistently described using the porosity-to-volumetric cement content index (η/C_{iv}), as originally proposed by Consoli et al. (2007, 2010, 2019). As shown in Figure 2, the unconfined compressive strength (q_u) collapses into a unique trend when plotted against $\eta/C_{iv}^{0.16}$, despite the wide range of dry unit weights and cement contents investigated.

This convergence demonstrates that η/C_{iv} effectively normalises the combined effects of porosity and cement content on the strength of the iron ore tailings–OPC blends. The dashed line in Figure 2 indicates the operational strength limit of the true triaxial apparatus ($q_u \approx 180$ kPa corresponding to $\eta/C_{iv}^{0.16} \approx 42.40$), which guided the selection of mixtures for Phase II. As expected, lower porosity and higher cement content increased q_u, confirming the effectiveness of the cementitious matrix within the investigated dosage range.

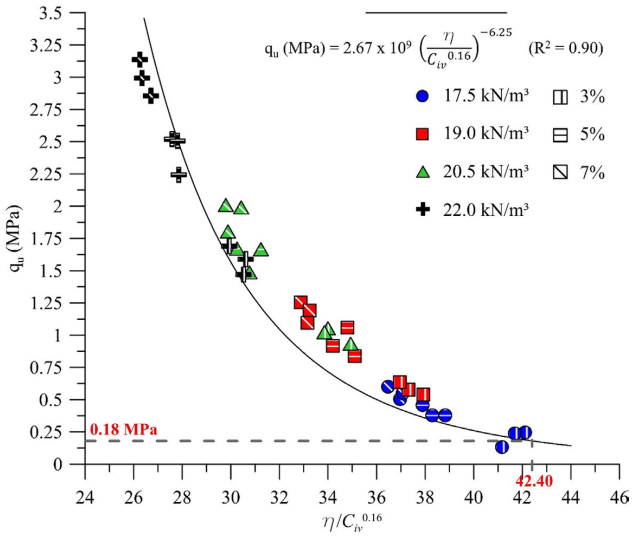


Figure 2. Iron ore tailings-ordinary Portland cement unconfined compressive strength in function of the porosity/volumetric cement content index ($\eta/C_{iv}^{0.16}$).

5.2 True triaxial test results

True triaxial tests were conducted on both untreated and OPC-treated specimens for $b = 0$, 0.5, and 1, with results analysed by loading angle (θ). Untreated tailings exhibited substantially higher strain magnitudes than cemented specimens, particularly at small to intermediate stress ratios.

For $b = 0$ (Figure 3), OPC treatment increased stiffness markedly, by a factor of at least 2.5 relative to untreated material, while strength gains were more modest, rising from $q \approx 130$ kPa to $q \approx 170$ kPa. This indicates that, under the mean effective stress adopted ($p' = 100$ kPa), the cementitious matrix primarily enhances elastic response rather than ultimate strength, consistent with limited damage to the bonding network during loading.

Notably, the $\eta/C_{iv}^{0.16}$ value used to select Phase II mixtures (≈ 42.40) yielded triaxial strengths closely matching the target unconfined strength (180 kPa) for the $\theta = 0°$ path, which mimics axial compression. This agreement reinforces the index's applicability beyond uniaxial conditions, suggesting its potential as a unified design parameter for predicting performance under varied stress paths. The differences in stiffness and strain behaviour between treated and untreated specimens also set the stage for analysing how cementation influences anisotropy, as explored in the following sections.

In laboratory-prepared sandy soils, cross-anisotropy is commonly induced by the compaction process, with the horizontal plane tending toward isotropy (Parkin et al., 1968; Arthur & Menzies, 1972; Oda & Koishikawa, 1979; Fioravante & Capoferri, 2001). A similar pattern was observed for the untreated specimens. In the ($b = 0$) tests, the $\theta = 0°$

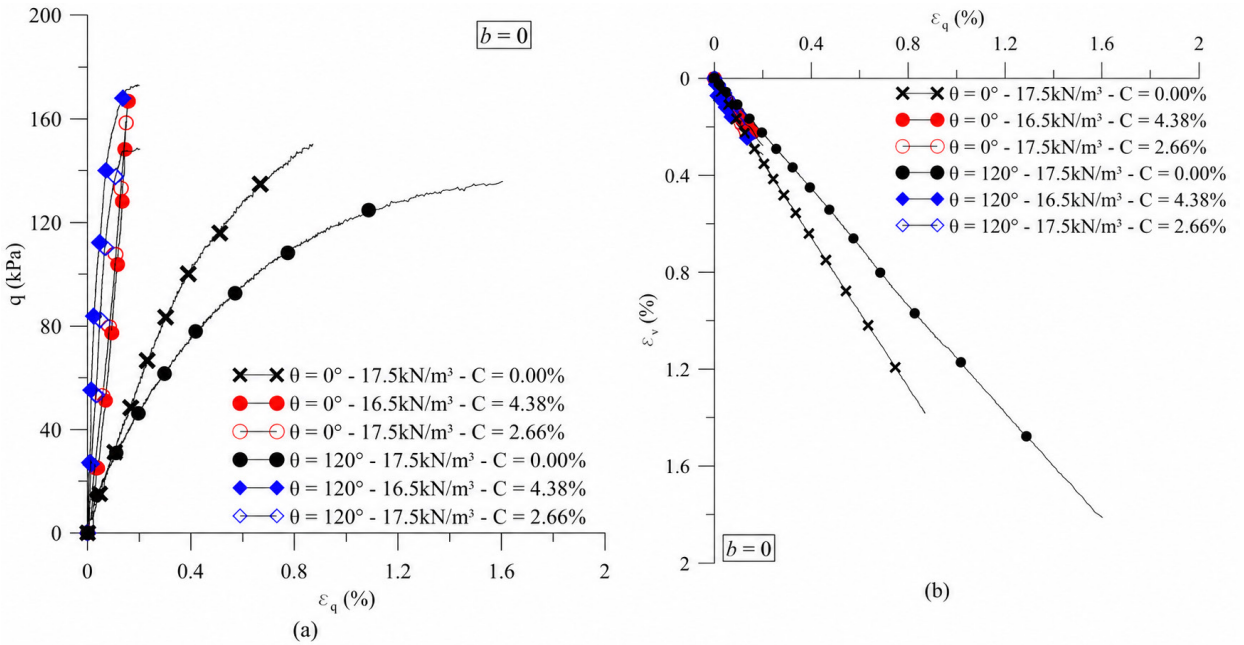


Figure 3. Intermediate stress parameter $b = 0$ stress versus (a) deviatoric strain and (b) volumetric strain.

loading path, in which σ_1 was aligned with the compaction Z-axis, resulted in greater stiffness than the $\theta = 120°$ path, in which σ_1 was aligned with the Y-axis (see Figure 3a, untreated specimens). This response is consistent with the influence of compaction-induced fabric anisotropy.

For OPC-treated specimens, the stiffness difference between $\theta = 0°$ and $\theta = 120°$ was substantially reduced within the 0–0.15% strain range. The $\theta = 120°$ path was occasionally marginally stiffer, indicating that cementation modified the directional response. However, the remaining differences indicate only partial anisotropy suppression. Similar reductions have been reported for other cemented granular materials (Festugato et al., 2013, 2019, 2023; Silvani, 2017; Silvani et al., 2022), likely because the cementitious matrix reinforces particle contacts in all directions without fully eliminating the initial fabric.

Figure 3b shows the volumetric–deviatoric strain response for $b = 0$. Untreated specimens reached compressive volumetric strains of approximately 2%, reflecting the contractive behaviour of fine-grained tailings under axial compression, whereas OPC-treated specimens remained below 0.4%. Cementation therefore reduced the contractive response associated with pore-pressure build-up and liquefaction susceptibility, even at cement contents of 2.66% and 4.38%. Increased compaction remains a complementary means of reducing voids when feasible.

The trend observed for $b = 0$ extended to $b = 0.5$. Figure 4 presents the corresponding stress–strain and deviatoric–volumetric strain relationships. Plane-stress specimens exhibited higher stiffness, with strains below approximately 0.075%. For $b = 0.5$ ($\theta = 30°$, 90° and 150°), σ_2 remained constant while σ_1 increased and σ_3 decreased proportionally, resulting in limited ε_2 variation. This restricted intermediate-direction deformation may have contributed to the increased stiffness.

Lade & Duncan (1973) similarly reported larger strains to failure under $b = 0$ than under $b = 0.5$, indicating that the reduced strain range and higher stiffness observed here agree with established multiaxial behaviour. In cemented iron ore tailings, the interaction between cementation and constant intermediate principal stress may further increase stiffness and delay volumetric instability relative to axisymmetric compression.

The higher stiffness at $\theta = 30°$ likely reflects alignment of σ_1 with the compaction Z-axis, allowing the initial fabric to contribute directly to resistance. At $\theta = 90°$, σ_1 acts along Y, σ_3 unloading occurs along Z and σ_2 remains constant along X, partially preserving the Z-axis fabric effect and producing intermediate stiffness. At $\theta = 150°$, σ_1 and σ_3 act along Y and X, respectively, without direct loading of Z, reducing the fabric contribution and stiffness. Thus, residual anisotropy may persist in cemented specimens when the loading path does not mobilise the primary compaction direction.

Figure 4b shows that $b = 0.5$ specimens developed approximately half the volumetric strain recorded for $b = 0$, indicating lower contractive tendency. Lade & Duncan (1975) noted that increasing b generally reduces axial strain at failure, consistent with the trend observed from $b = 0$ to 0.5 and 1. Plane-stress conditions therefore promote volumetric stability, while cementation combined with constant σ_2 further suppresses volumetric strain and enhances resistance to contractive instability.

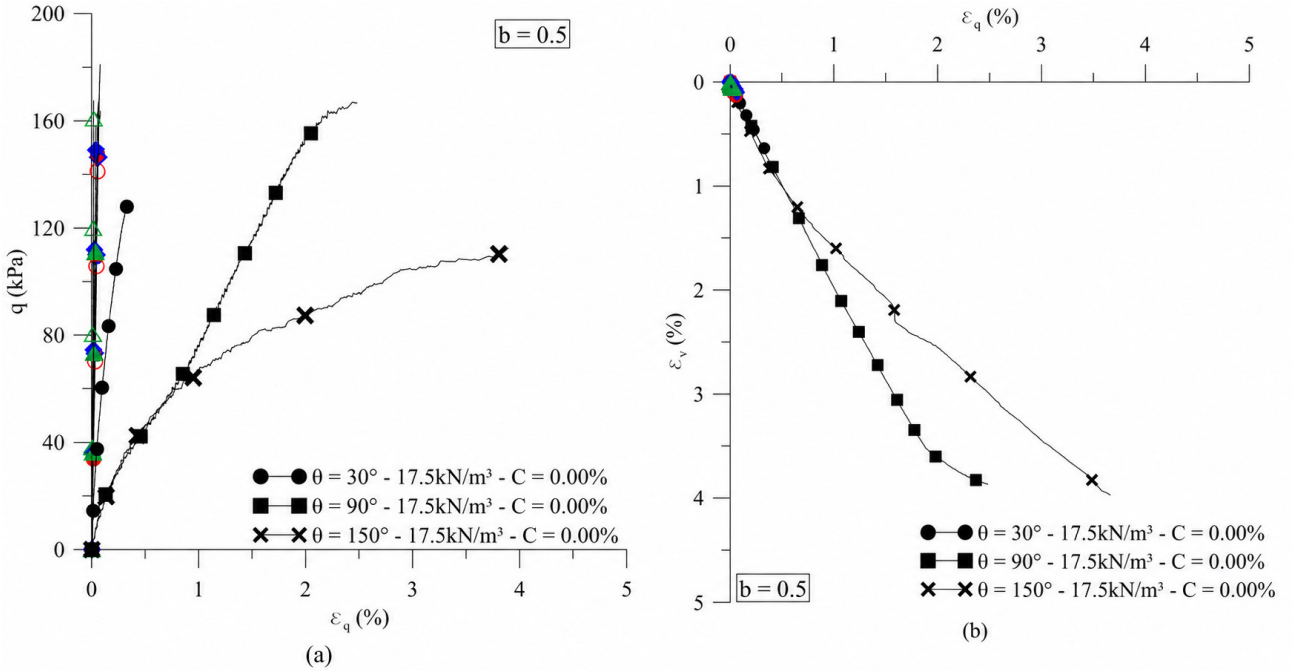


Figure 4. Intermediate stress parameter $b = 0.5$ stress (a) deviatoric strain and (b) volumetric strain.

Figure 5a shows the deviatoric stress–deviatoric strain curves for $b = 1$ tests. Consistent with Festugato et al. (2023) and Andreghetto et al. (2022), the true triaxial extension paths produced the lowest strengths among all loading conditions, reflecting the severity of this stress path where σ_2 equals σ_1. For untreated specimens, $b = 1$ results also revealed cross-sectional anisotropy linked to the Z-axis compaction direction. In the $\theta = 60°$ path, loading is applied to both Y and Z-axes while the X-axis is progressively unloaded. Mobilization of the Z-axis fabric in this configuration results in higher stiffness compared to $\theta = 180°$, where loading occurs along the X and Y-axes and the Z-axis is unloaded. The absence of Z-axis mobilization in $\theta = 180°$ likely accounts for the substantial stiffness reduction observed in this path.

Figure 5b presents the volumetric strain behaviour for $b = 1$ specimens. An increased dilation rate is observed when compared to $b = 0$ results, consistent with the observations of Lade & Duncan (1975) and Reddy & Saxena (1993). These authors also reported that $b = 1$ conditions tend to produce greater overall volumetric strain, a trend confirmed in the present study. In the context of cemented iron ore tailings, this indicates that even with cementation, extension-dominated stress paths can mobilize more significant volumetric changes, highlighting a potential limitation of cement stabilization under high-b conditions.

Figure 6 presents the $b = 0$ true triaxial test results, with Figure 6a showing the $\theta = 0°$ loading path and Figure 6b the $\theta = 120°$ path. The stress–strain curves for both dosages tested ($\gamma_d = 16.5$ kN/m³ – $C = 4.38\%$ and $\gamma_d = 17.5$ kN/m³ – $C = 2.66\%$) are nearly identical, regardless of the loading axis, reaffirming the robustness of the $\eta/C_{iv}^{0.16}$ index as a unifying parameter. This equivalence indicates that once the target index value is reached, the influence of the specific cement–porosity combination becomes secondary in determining global mechanical response.

In the $\theta = 0°$ path, the Z-axis acts as the major principal stress direction, which in anisotropic specimens would typically produce larger strains due to mobilization of the primary compaction fabric. Here, however, ε_2 and ε_3 show similar magnitudes and trends, suggesting cross-sectional isotropy. The same holds for $\theta = 120°$, where the major principal stress acts along the Y-axis. The equivalence in deviatoric stress–strain behaviour between $\theta = 0°$ and $\theta = 120°$ further supports the conclusion that compaction-induced anisotropy has been largely neutralized by cementation.

This convergence between orthogonal loading directions suggests that the cementitious bonds have established a three-dimensional load transfer network that overrides the directional contact orientation imparted during compaction. In practical terms, this means that for design purposes, once an adequate $\eta/C_{iv}^{0.16}$ threshold is achieved, the orientation of field loading relative to the deposition fabric may have a reduced influence on performance, potentially simplifying stability analyses for "dry"-stacked tailings where deposition layers are not perfectly aligned with operational loading paths.

Figure 7 presents the $b = 0.5$ test results, in which two principal stress axes are loaded while the third remains constant at the same magnitude. The stress–strain curves for both dosages tested are essentially identical, indicating that, within the tested range, the cement–porosity combination does not significantly affect the global response under plane stress conditions.

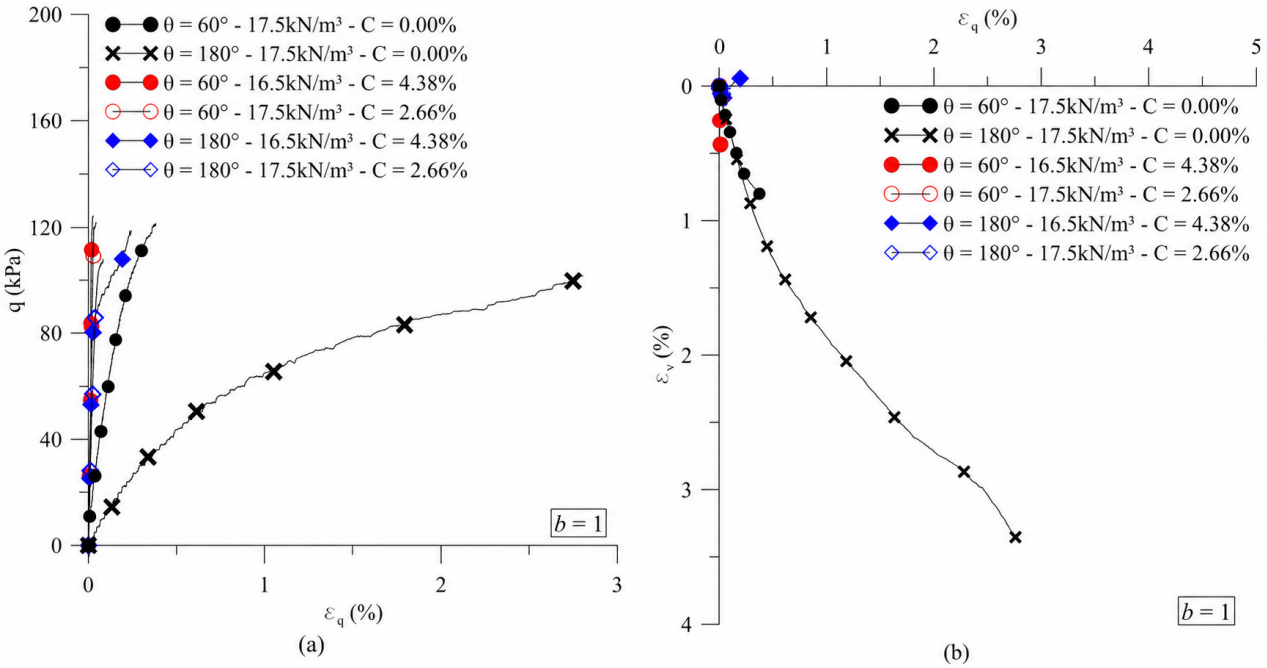


Figure 5. Intermediate stress parameter $b = 1$ stress versus the (a) deviatoric strain and (b) volumetric strain.

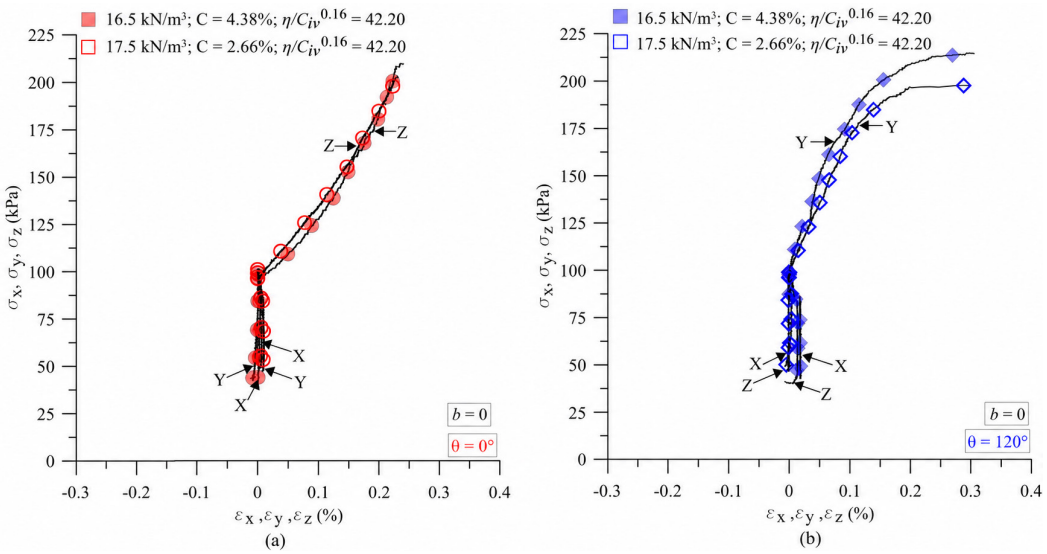


Figure 6. X, Y and Z stress versus strain for $b = 0$: (a) $\theta = 0°$; and (b) $\theta = 120°$.

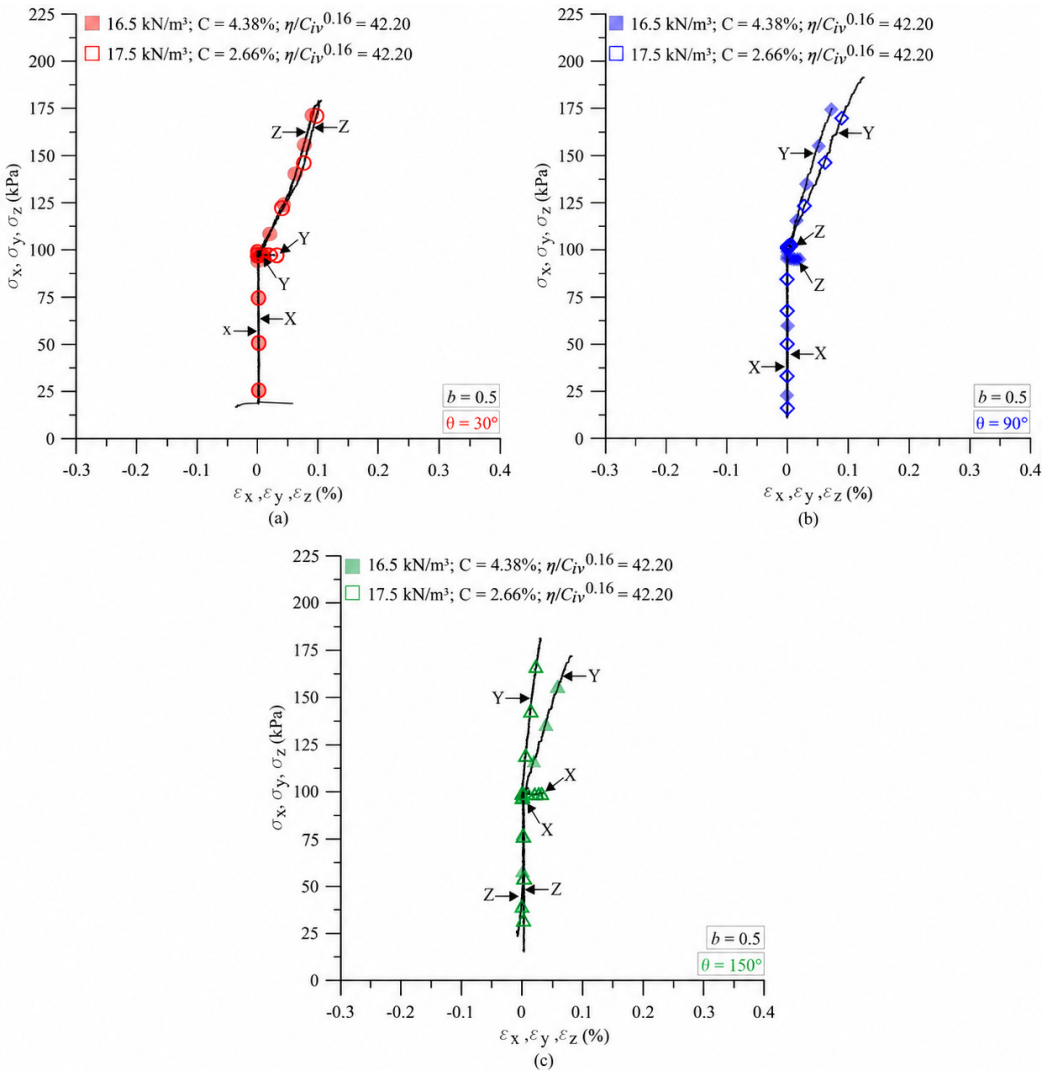


Figure 7. X, Y and Z stress versus strain for $b = 0.5$: (a) $\theta = 30°$; (b) $\theta = 90°$, and c) $\theta = 150°$.

The results reveal no discernible influence of compaction-induced anisotropy. Both strain magnitudes and σ_1 values were similar for θ = 30°, 90°, and 150°, despite the different loading orientations. Although σ_1 was aligned with the compaction Z-axis at θ = 30° and with the Y-axis at θ = 90° and 150°, the θ = 30° path exhibited no appreciable stiffness or strength advantage. This convergence indicates that cementation largely suppressed, or possibly eliminated, the mechanical effects of the compaction-induced fabric.

The absence of anisotropic response under b = 0.5 implies that when σ_2 is held constant, the influence of initial deposition fabric is less critical, even in untreated soils. Cementation further reinforces this effect, producing a homogenized response across different loading orientations. For engineering applications, this could mean that in structures subjected predominantly to plane stress states, such as certain zones in "dry"-stacked tailings piles, the required cement dosage to mitigate anisotropy-related performance variability may be lower than for axisymmetric loading conditions.

Figure 8 shows the b = 1 test results, where isotropic behaviour is again evident, particularly for the γ_d = 17.5 kN/m^3, C = 2.66% specimen. Lade & Duncan (1973) reported that for untreated sands, the method of deposition had little influence on behaviour, with specimens approaching isotropy under certain conditions. Silvani et al. (2022) observed a similar trend in Osorio sand–fly ash–lime blends, attributing it to the cementation effect reducing preparation-induced anisotropy. Likewise, Andreghetto (2022) reported that in Osorio sand–OPC blends, anisotropy decreased with increasing cement content within a range (0 – 2.14%) comparable to that used in this study.

In contrast, Festugato et al. (2019, 2023) found that light cementation (1.8% and 2.3% OPC) in Hostun RF sand was insufficient to erase compaction-induced anisotropy. The present results, together with these studies, indicate that the extent to which cementation can neutralize anisotropy depends strongly on particle shape, grading, and surface roughness, in addition to binder content. Figure 8b further confirms isotropy in the present cemented tailings, as X- and Y-axis load responses are nearly identical throughout the test.

The ability of low cement contents to promote isotropy in fine-grained, angular iron ore tailings, contrary to the behaviour observed in some sands, suggests that particle morphology and surface area may enhance the effectiveness of cement bridges in distributing stresses more uniformly. This points to a material-specific interaction between cementation and initial fabric, implying that binder dosages required for anisotropy mitigation should be tailored not only to target strength but also to the mineralogical and morphological characteristics of the tailings.

Isotropy is further supported by the similarity in q_{max} for tests conducted at the same intermediate stress parameter b, regardless of loading orientation. This alignment between $\eta/Civ^{0.16}$, unconfined compression, and multiaxial loading outcomes suggests that the index could serve not only as a mix design tool but also as a performance predictor under varied stress states. Such cross-condition predictability is valuable for field applications, where stress paths can differ significantly across zones of a tailings facility, allowing engineers to calibrate compaction and cementation targets with a single unified parameter.

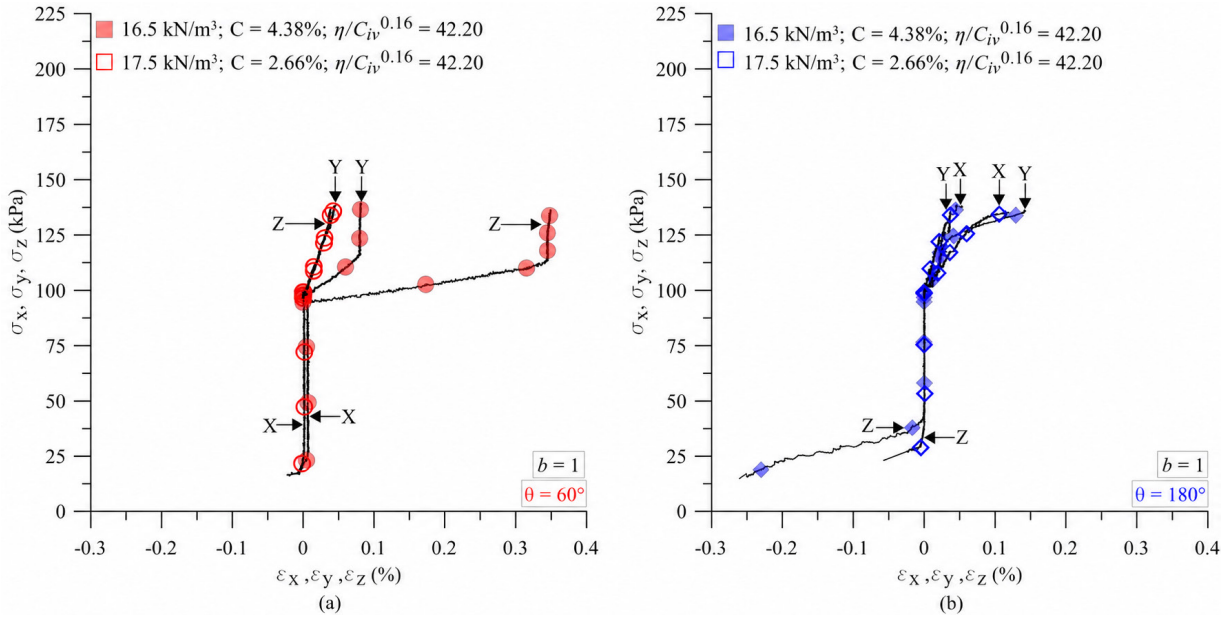


Figure 8. X, Y and Z stress versus strain for b = 1: (a) θ = 60°; and (b) θ = 180°.

Figure 9 shows the peak deviatoric stresses for each true triaxial test plotted against loading angle θ. The uncemented specimens follow the pattern reported by Corte et al. (2019), Corte (2020) and Andreghetto (2022), where $b = 0$ ($\sigma_2 = \sigma_3$) conditions yield the highest strengths, $b = 0.5$ (constant σ_2) produce intermediate strengths, and $b = 1$ ($\sigma_2 = \sigma_1$) generate the lowest strengths.

For the cemented specimens, represented by the red circular and triangular symbols in Figure 9, this strength hierarchy changes. The strengths obtained under ($b = 0$) and ($b = 0.5$) are nearly identical, indicating that cementation substantially reduced the influence of the intermediate principal stress on strength under compression and plane-stress conditions. This convergence suggests a partial suppression of strength anisotropy within this range of loading conditions. Once a continuous cementitious network develops, the load-bearing capacity appears to become less sensitive to variations in σ_2 across the compression–plane-stress spectrum. From a design perspective, this reduced sensitivity may facilitate strength prediction and could potentially limit the need for extensive stress-path-specific testing, although further validation would be required before adopting a single representative strength value.

Figure 9 also demonstrates the benefits of OPC stabilisation, with substantial strength gains observed along most loading paths. Its effectiveness was more limited, however, for the tensile-dominated paths at $\theta = 60°$ and 180°, for which the cemented and untreated specimens attained similar strengths. This suggests that, at the cement contents investigated, the mechanisms governing tensile-dominated failure were not substantially modified by cementation. Moreover, the red circular and triangular symbols converge towards a similar deviatoric stress despite differences in cement content and loading path, further supporting the predictive capability of the $\eta/Civ^{0.16}$ parameter across the investigated conditions.

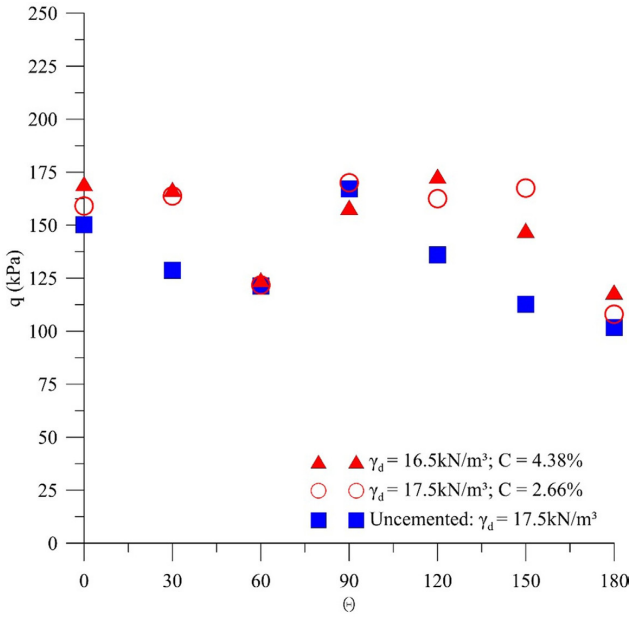


Figure 9. Deviatoric stress – q (kPa) in function of the θ loading angle.

6. Practical application

The practical contribution of this study is to connect cement–porosity-based mixture selection with the mechanical response expected under different loading directions and stress paths in filtered-tailings stacks. The comparable responses of the two investigated mixtures indicate that, within the tested conditions, a lower achievable dry density can be compensated by a higher cement content, providing alternatives for treating loosely compacted zones or adapting mixture specifications to field compaction capabilities. Beyond achieving a target unconfined compressive strength, the results show that cementation can improve stiffness, reduce contractive deformation and diminish the directional dependence introduced by layer compaction, supporting its use where deformation control and more uniform mechanical performance are required. The measured stress–strain responses can also support the calibration and assessment of constitutive models for stack deformation and stability analyses. Importantly, the distinction between reduced fabric anisotropy and persistent stress-path dependency helps guide parameter selection: the similar strengths under compression and intermediate-stress conditions suggest that a common strength representation may be investigated for these paths, whereas extension-dominated conditions require separate consideration. For different tailings, stack heights or disposal practices, this approach can be extended by calibrating the porosity–cement relationship for the local material and testing selected mixtures at effective stresses and preparation conditions representative of the intended application, thereby translating laboratory mixture selection into field-specific performance criteria.

7. Conclusions

The present study investigated the multiaxial response of lightly cemented iron ore tailings under different intermediate principal stress conditions and loading orientations. The main conclusions are as follows:

1. The $\eta/C_{iv}^{0.16}$ index provided a consistent basis for selecting mixtures for multiaxial testing. At the investigated value of $\eta/C_{iv}^{0.16} \approx 42.40$, mixtures prepared with different dry unit weights and cement contents achieved similar unconfined compressive strengths and comparable multiaxial responses, particularly under $b = 0$ and $b = 0.5$ conditions.
2. Cementation markedly increased stiffness and reduced volumetric strains relative to the untreated tailings. It also substantially reduced the directional differences associated with the compaction-induced fabric, with the clearest reduction in anisotropy occurring under compression and plane-stress conditions ($b = 0$ and $b = 0.5$).

3. Extension-dominated loading paths ($b = 1$) produced the lowest peak strengths and more pronounced volumetric changes. The benefits of cementation were less marked under these conditions, demonstrating that stress-path dependency remains relevant even when the initial fabric anisotropy is reduced.
4. The similarity between the responses obtained for orthogonal loading directions indicates that cementitious bonding can reduce the influence of the compaction direction on the multiaxial behaviour of iron ore tailings. However, because the study investigated a single target $\eta/C_{iv}^{0.16}$ value and mean effective stress, further testing is required before defining a general threshold or binder dosage for anisotropy mitigation. Binder selection should therefore consider both the target strength and the stress paths expected in the field.

Acknowledgements

The authors wish to express their gratitude to the Brazilian National Council for Technology Development – (CNPq) for supporting the research group (grant number: 307286/2022-3 and 402572/2021-1) and the Fulbright program for the doctoral research awards as well.

Declaration of interest

The authors have no conflicts of interest to declare. All co-authors have observed and affirmed the contents of the paper and there is no financial interest to report.

Authors' contributions

Gustavo Dias Miguel: conceptualization, methodology, investigation, formal analysis, data curation, visualization, writing – original draft. Vinícius Batista Godoy: methodology, investigation, formal analysis, validation, writing - reviewing and editing. Lucas Festugato: conceptualization, supervision, funding acquisition, project administration, resources, writing - reviewing and editing.

Data availability

All data produced or examined in the course of the current study are included in this article.

Declaration of use of generative artificial intelligence

This work was prepared with the assistance of generative artificial intelligence (GenAI) ChatGPT, developed by OpenAI, with the aim of assist with language refinement, conciseness, and formatting. The entire process of using this tool was supervised, reviewed and when necessary edited by the authors. The authors assume full responsibility for the content of the publication that involved the aid of GenAI.

List of symbols and abbreviations

b	Intermediate principal stress parameter, $b = (\sigma_2 - \sigma_3)/(\sigma_1 - \sigma_3)$
p'	Mean effective stress (kPa)]
pH	Potential of Hydrogen
q	Deviatoric stress (kPa)
q_{max}	Peak deviatoric stress (kPa)
q_u	Unconfined compressive strength (kPa)
C	Cement content by dry mass of tailings (%)
C_{iv}	Volumetric cement content, expressed relative to the total specimen volume (%)
CL	Low-plasticity clay
CP	V-ARI High-early-strength Portland cement
D_{50}	Median particle diameter (mm)
OPC	Ordinary Portland cement
R^2	Coefficient of determination
UCS	Unconfined compressive strength
X, Y, Z	Orthogonal specimen axes, with the Z-axis aligned with the compaction direction
γ_d	Dry unit weight (kN/m^3)
ε_1	Principal strain associated with the major principal stress (%)
ε_2	Principal strain associated with the intermediate principal stress (%)
ε_3	Principal strain associated with the minor principal stress (%)
εs	Deviatoric strain (%)
εv	Volumetric strain (%)
εx	Normal strain along the specimen X-axis (%)
εy	Normal strain along the specimen Y-axis (%)
εz	Normal strain along the specimen Z-axis (%)
η	Porosity (%)
$\eta/C_{iv}^{0.16}$	Porosity-to-volumetric cement content index
σ_1	Major principal effective stress (kPa)
σ_2	Intermediate principal effective stress (kPa)
σ_3	Minor principal effective stress (kPa)
σ_x	Normal effective stress along the specimen X-axis (kPa)
σ_y	Normal effective stress along the specimen Y-axis (kPa)
σ_z	Normal effective stress along the specimen Z-axis (kPa)
θ	Loading direction on the deviatoric plane, expressed as the Lode angle (°)

References

ABNT NBR 5733. (2018). *Cimento Portland de alta resistência inicial*. ABNT - Associação Brasileira de Normas Técnicas, Rio de Janeiro, RJ (in Portuguese).

Andreghetto, D.H. (2022). *Comportamento de areias cimentadas artificialmente sob tensão multiaxial* [Doctoral thesis]. Universidade Federal do Rio Grande do Sul (in Portuguese).

Andreghetto, D.H., Festugato, L., Miguel, G.D., & da Silva, A. (2022). Automated true triaxial apparatus development for soil mechanics investigation. *Soils and Rocks*, 45(2), 1-10. https://doi.org/10.28927/SR.2022.077321.

Arthur, J.R.F., & Menzies, B.K. (1972). Inherent anisotropy in a sand. *Geotechnique*, 22(1), 115-128. https://doi.org/10.1680/geot.1972.22.1.115.

ASTM C150/C150M-12. (2012). *Standard specification for Portland cement*. ASTM International, West Conshohocken, PA. https://doi.org/10.1520/C0150_C0150M-12.

ASTM D854-14. (2014). *Standard test methods for specific gravity of soil solids by water pycnometer*. ASTM International, West Conshohocken, PA. https://doi.org/10.1520/D0854-14.

ASTM D4254-16. (2016). *Standard test methods for minimum index density and unit weight of soils and calculation of relative density*. ASTM International, West Conshohocken, PA. https://doi.org/10.1520/D4254-16.

ASTM D4972-19. (2019). *Standard test methods for pH of soils*. ASTM International, West Conshohocken, PA. https://doi.org/10.1520/D4972-19.

ASTM C39/C39M-21. (2021a). *Standard test method for compressive strength of cylindrical concrete specimens*. ASTM International, West Conshohocken, PA. https://doi.org/10.1520/C0039_C0039M-21.

ASTM D1557-12(2021). (2021b). *Standard test methods for laboratory compaction characteristics of soil using modified effort (56,000 ft-lbf/ft3 [2,700 kN-m/m3])*. ASTM International, West Conshohocken, PA. https://doi.org/10.1520/D1557-12R21.

ASTM D2487-17. (2017a). *Standard practice for classification of soils for engineering purposes (Unified Soil Classification System)*. ASTM International, West Conshohocken, PA. https://doi.org/10.1520/D2487-17.

ASTM D4318-17. (2017b). *Standard test methods for liquid limit, plastic limit, and plasticity index of soils*. ASTM International, West Conshohocken, PA. https://doi.org/10.1520/D4318-17.

ASTM D6913/D6913M-17. (2017c). *Standard test methods for particle-size distribution (gradation) of soils using sieve analysi*s. ASTM International, West Conshohocken, PA. https://doi.org/10.1520/D6913_D6913M-17.

Carretta, M.S., Cristelo, N., Festugato, L., Miguel, G.D., & Consoli, N.C. (2020). Experimental assessment of the small-strain response of residual soil under monotonic and cyclic loading. *Proceedings of the Institution of Civil Engineers - Geotechnical Engineering*, 175(6), 556-569. https://doi.org/10.1680/jgeen.20.00073.

Consoli, N.C., Foppa, D., Festugato, L., & Heineck, K.S. (2007). Key parameters for strength control of artificially cemented soils. *Journal of Geotechnical and Geoenvironmental Engineering*, 133(2), 197-205. https://doi.org/10.1061/(ASCE)1090-0241(2007)133:2(197).

Consoli, N.C., Cruz, R.C., Floss, M.F., & Festugato, L. (2010). Parameters controlling tensile and compressive strength of artificially cemented sand. *Journal of Geotechnical and Geoenvironmental Engineering*, 136(5), 759-763. https://doi.org/10.1061/(ASCE)GT.1943-5606.0000278.

Consoli, N.C., Dalla Rosa, A., & Saldanha, R.B. (2011). Variables governing strength of compacted soil-fly ash-lime mixtures. *Journal of Materials in Civil Engineering*, 23(4), 432-440. https://doi.org/10.1061/(ASCE)MT.1943-5533.0000186.

Consoli, N.C., Samaniego, R.A.Q., & Villalba, N.M.K. (2016). Durability, strength, and stiffness of dispersive clay-lime blends. *Journal of Materials in Civil Engineering*, 28(11), 04016124. https://doi.org/10.1061/(ASCE)MT.1943-5533.0001632.

Consoli, N.C., Silva, A., Barcelos, A.M., Festugato, L., & Favretto, F. (2019). Porosity/cement index controlling flexural tensile strength of artificially cemented soils. *Geotechnical and Geological Engineering*, 38(1), 713-722. https://doi.org/10.1007/s10706-019-01059-w.

Consoli, N.C., Festugato, L., Scheuermann Filho, H.C., Miguel, G.D., Tebechrani Neto, A., & Andreghetto, D. (2020a). Durability assessment of soil-pozzolan-lime blends through ultrasonic-pulse velocity test. *Journal of Materials in Civil Engineering*, 32(8), 04020223. https://doi.org/10.1061/(ASCE)MT.1943-5533.0003298.

Consoli, N.C., Moreira, E.B., Festugato, L., & Miguel, G.D. (2020b). Spread footings bearing on circular and square cement-stabilized sand layers above weakly bonded residual soil. *Soils and Rocks*, 43(3), 339-349. https://doi.org/10.28927/SR.433339.

Consoli, N.C., Festugato, L., Miguel, G.D., Moreira, E.B., & Scheuermann Filho, H.C. (2021a). Fatigue life of green stabilized fiber-reinforced sulfate-rich dispersive soil. *Journal of Materials in Civil Engineering*, 33(9), 04021249. https://doi.org/10.1061/(ASCE)MT.1943-5533.0003842.

Consoli, N.C., Festugato, L., Miguel, G.D., & Scheuermann Filho, H.C. (2021b). Swelling prediction for green stabilized fiber-reinforced sulfate-rich dispersive soils. *Geosynthetics International*, 28(4), 391-401. https://doi.org/10.1680/jgein.20.00050.

Consoli, N.C., Vogt, J.C., Silva, J.P.S., Chaves, H.M., Scheuermann Filho, H.C., Moreira, E.B., & Lotero, A. (2022). Behaviour of compacted filtered iron ore tailings-Portland cement blends: new Brazilian trend for tailings disposal by stacking. *Applied Sciences (Basel, Switzerland)*, 12(2), 836. https://doi.org/10.3390/app12020836.

Corte, M.B. (2020). Response of lightly cemented sand under multiaxial loading [Doctoral thesis]. Universidade Federal do Rio Grande do Sul. Retrieved in July 18, 2026, from http://hdl.handle.net/10183/212194.

Corte, M.B., Ibraim, E., Festugato, L., Diambra, A., & Consoli, N.C. (2019). Stiffness of lightly cemented sand under multiaxial loading. *E3S Web of Conferences*, 92, 11008. https://doi.org/10.1051/e3sconf/20199211008.

Davies, M.P., Lupo, J., Martin, T., McRoberts, E., Musse, M., & Ritchie, D. (2011). Dewatered tailings practice: trends and observations. In *Proceedings of the Tailings and Mine Waste 2010* (pp. 133-142). CRC Press. https://doi.org/10.1201/b10569-19.

Dutra, M.R. (2021). *Comportamento geomecânico de um rejeito de minério de ferro para baixas e altas tensões de confinamento* [Dissertação de mestrado]. Universidade Federal do Rio Grande do Sul (in Portuguese).

Festugato, L., Consoli, N.C., & Fourie, A. (2015). Cyclic shear behaviour of fibre-reinforced mine tailings. *Geosynthetics International*, 22(2), 196-206. https://doi.org/10.1680/gein.15.00005.

Festugato, L., Corte, M.B., Ibraim, E., & Diambra, A. (2019). Artificially cemented sand under multiaxial loading. *E3S Web of Conferences*, 92, 11011. https://doi.org/10.1051/e3sconf/20199211011.

Festugato, L., Fourie, A., & Consoli, N.C. (2013). Cyclic shear response of fibre-reinforced cemented paste backfill. *Géotechnique Letters*, 3(1), 5-12. https://doi.org/10.1680/geolett.12.00042.

Festugato, L., Ibraim, E., Corte, M.B., & Diambra, A. (2023). Multiaxial behaviour of compacted artificially lightly cemented sands. *Journal of Geotechnical and Geoenvironmental Engineering*, 149(12), 04023118. https://doi.org/10.1061/JGGEFK.GTENG-11389.

Figueredo, M.M. (2007). *Estudo de metodologias alternativas de disposição de rejeitos para a mineração Casa de Pedra - Congonhas/MG* [Master's dissertation]. Universidade Federal de Ouro Preto (in Portuguese).

Fioravante, V., & Capoferri, R. (2001). On the use of multidirectional piezoelectric transducers in triaxial testing. *Geotechnical Testing Journal*, 24(3), 243-255. https://doi.org/10.1520/GTJ11344J.

Guerra, F. (1973). Characteristics of tailings from a soils engineer's viewpoint. In C. Aplin & G. Argall (Eds.), *Proceedings of the 1st International Tailing Symposium* (pp. 102-137). Miller Freeman.

Guerra, F. (1979). Controlling the phreatic surface. In G. Argall (Ed.), *Proceedings of the 2nd International Tailing Symposium* (pp. 292-326). Miller Freeman.

Instituto Brasileiro de Mineração – IBRAM. (2020). *Economia mineral: Fevereiro de 2020*. Instituto Brasileiro de Mineração (in Portuguese).

Klohn, E. (1979). Taconite tailings disposal practices. In American Society of Civil Engineers. Committee on Embankment Dams and Slopes. *Current geotechnical practice in mine waste disposal* (pp. 202-241). American Society of Civil Engineers.

Kossoff, D., Dubbin, W.E., Alfredsson, M., Edwards, S.J., Macklin, M.G., & Hudson-Edwards, K.A. (2014). Mine tailings dams: characteristics, failure, environmental impacts, and remediation. *Applied Geochemistry*, 51, 229-245. https://doi.org/10.1016/j.apgeochem.2014.09.010.

Lade, P.V., & Duncan, J.M. (1973). Cubical triaxial tests on cohesionless soil. *Journal of the Soil Mechanics and Foundations Division*, 99(10), 793-812. https://doi.org/10.1061/JSFEAQ.0001934.

Lade, P.V., & Duncan, J.M. (1975). Elastoplastic stress-strain theory for cohesionless soil. *Journal of the Geotechnical Engineering Division*, 101(10), 1037-1053. https://doi.org/10.1061/AJGEB6.0000204.

Li, W., & Coop, M.R. (2019). Mechanical behaviour of Panzhihua iron tailings. *Canadian Geotechnical Journal*, 56(3), 420-435. https://doi.org/10.1139/cgj-2018-0032.

Lupo, J., & Hall, J. (2010). Dry stack tailings: design considerations. In *Proceedings of the 14th International Conference on Tailings and Mine Waste*. CRC Press.

Menger, E.S., da Silva, A., & Festugato, L. (2022). Mechanical behavior of a fiber reinforced reclaimed asphalt pavement sand-cement blend. *Geosynthetics International*, 29(5), 520-533. https://doi.org/10.1680/jgein.21.00064.

Miguel, G.D., Festugato, L., Moreira, E.B., & Corte, M.B. (2021). Discussion of "Geopolymers based on recycled glass powder for soil stabilization" by Jair de Jesús Arrieta Baldovino, Ronaldo dos Santos Izzo, Juliana Lundgren Rose, and Mônica Angélica Avanci. *Geotechnical and Geological Engineering*, 39(6), 4649-4653. https://doi.org/10.1007/s10706-021-01762-7.

Miguel, G.D., Festugato, L., Scheuermann Filho, H.C., & Daronco, J.V.L. (2022a). Discussion of "Fiber-reinforced cement-stabilized macadam with various polyvinyl alcohol fiber contents and lengths" by Chunhua Zhao, Naixing Liang, Xiaolong Zhu, Lingqing Yuan, and Bo Zhou. *Journal of Materials in Civil Engineering*, 34(3), 07021019. https://doi.org/10.1061/(ASCE)MT.1943-5533.0004291.

Miguel, G.D., Festugato, L., Daronco, J.V.L., & da Silva, A. (2022b). Discussion of "Triaxial axis shear mechanical properties of fiber-reinforced foamed lightweight soil" by Xu Jiangbo, Luo Yongzhen, Wang Yuanzhi, Yan Changgen, Zhang Liujun, Yin Lihua, Yang Xiaohua, Qiu Youqiang, and Lan Hengxing. *Journal of Materials in Civil Engineering*, 34(11), 07022012. https://doi.org/10.1061/(ASCE)MT.1943-5533.0004472.

Miguel, G.D., Saldanha, R.B., da Silva, A., Festugato, L., Chaves, H.M., & Mendes, C.C. (2023). Comparison of life-cycle assessment: environmental and cost approach to soil improvement. *Proceedings of the Institution of Civil Engineers - Ground Improvement*, 176(3), 182-198. https://doi.org/10.1680/jgrim.21.00006a.

Ministry of Foreign Affairs of Brazil – MRE. (2021). *Business guide: Botswana*. Ministry of Foreign Affairs of Brazil.

Mitchell, J.K. (1981). Soil improvement: state-of-the-art report. In *Proceedings of the 10th International Conference on Soil Mechanics and Foundation Engineering* (Vol. 4, pp. 509-565). International Society for Soil Mechanics and Foundation Engineering.

CC BY

Morgenstern, N.R., Vick, S.G., Viotti, C.B., & Watts, B.D. (2016). *Fundão tailings dam review panel: Report on the immediate causes of the failure of the Fundão dam*. Cleary Gottlieb Steen & Hamilton LLP.

Oda, M., & Koishikawa, I. (1979). Effect of strength anisotropy on bearing capacity of shallow footing in a dense sand. *Soil and Foundation*, 19(3), 15-28. https://doi.org/10.3208/sandf1972.19.3_15.

Parkin, A.K., Gerrard, C.M., & Willoughby, D.R. (1968). Discussion of "Deformation of sand in hydrostatic compression". *Journal of the Soil Mechanics and Foundations Division*, 94(1), 336-340. https://doi.org/10.1061/JSFEAQ.0001094.

Pasche, E., Bruschi, G.J., Specht, L.P., Aragão, F.T.S., & Consoli, N.C. (2022). Fiber-reinforcement effect on the mechanical behavior of reclaimed asphalt pavement-powdered rock-Portland cement mixtures. *Transportation Engineering*, 10, 100121. https://doi.org/10.1016/j.treng.2022.100121.

Pereira, E.L. (2005). *Estudo do potencial de liquefação de rejeitos de minério de ferro sob carregamento estático* [Master's dissertation]. Universidade Federal de Ouro Preto (in Portuguese).

Queiroz, L.C., Miguel, G.D., Bruschi, G.J., & Lima, M.D.S. (2022). Macro-micro characterization of green stabilized alkali-activated sand. *Geotechnical and Geological Engineering*, 40(7), 3763-3778. https://doi.org/10.1007/s10706-022-02130-9.

Reddy, K.R., & Saxena, S.K. (1993). Effects of cementation on stress-strain and strength characteristics of sands. *Soil and Foundation*, 33(4), 121-134. https://doi.org/10.3208/sandf1972.33.4_121.

Rezende, V.A. (2013). *Estudo do comportamento de barragem de rejeito arenoso alteada por montante* [Master's dissertation]. Universidade Federal de Ouro Preto (in Portuguese).

Robertson, P.K., Melo, L., Williams, D.J., & Wilson, G.W. (2019). *Report of the expert panel on the technical causes of the failure of Feijão Dam I* . [s.n.].

Scheuermann Filho, H.C., Miguel, G.D., & Consoli, N.C. (2022a). Durability response of a cemented clayey sand over a wide range of porosities and cement contents. *Cleaner Materials*, 5, 100117. https://doi.org/10.1016/j.clema.2022.100117.

Scheuermann Filho, H.C., Miguel, G.D., & Consoli, N.C. (2022b). Porosity/cement index over a wide range of porosities and cement contents. *Journal of Materials in Civil Engineering*, 34(3), 06021011. https://doi.org/10.1061/(ASCE)MT.1943-5533.0004115.

Shukin, W., & Olsen, M. (1980). Quebec Cartier-Mount Wright tailings disposal. In *Symposium on Design and Construction of Tailings Dams*. Colorado School of Mines.

Silva, A., Festugato, L., Daronco, J.V.L., & Menger, E. (2022). Mechanical response of a sand, reclaimed asphalt pavement, and Portland cement mixture. *Journal of Materials in Civil Engineering*, 34(9), 04022213. https://doi.org/10.1061/(ASCE)MT.1943-5533.0004361.

Silvani, C. (2017). *Solos artificialmente cimentados em célula cúbica: isotropia a pequenas deformações e na ruptura* [Doctoral thesis]. Universidade Federal do Rio Grande do Sul (in Portuguese).

Silvani, C., Ibraim, E., Scheuermann Filho, H.C., Festugato, L., Diambra, A., & Consoli, N.C. (2022). Sand-fly ash-lime blends: mechanical behavior under multiaxial stress condition. *Journal of Materials in Civil Engineering*, 34(5), 04022059. https://doi.org/10.1061/(ASCE)MT.1943-5533.0004199.